Submitted to ADVANCED MATERIALS

Supporting Information for High-Moment Antiferromagnetic Nanoparticles with Tunable Magnetic Properties

Passivation and materials for SAF nanoparticles

The materials used here are selected based on their magnetic performance in read head sensors for magnetic disk drives. Ta is used to passivate the SAF nanoparticle surfaces, as shown in Fig. S1a and results in excellent chemical and magnetic stability in solution (Fig. S1b). The sidewall passivation by a thin layer of Ta_xO_y is a natural byproduct of ion-beam sputtering due to non-directional stray atom flux. It may be possible to obtain similar effects and stability for particles which are predominantly composed of iron or iron oxides, and therefore better suited to *in vivo* applications.

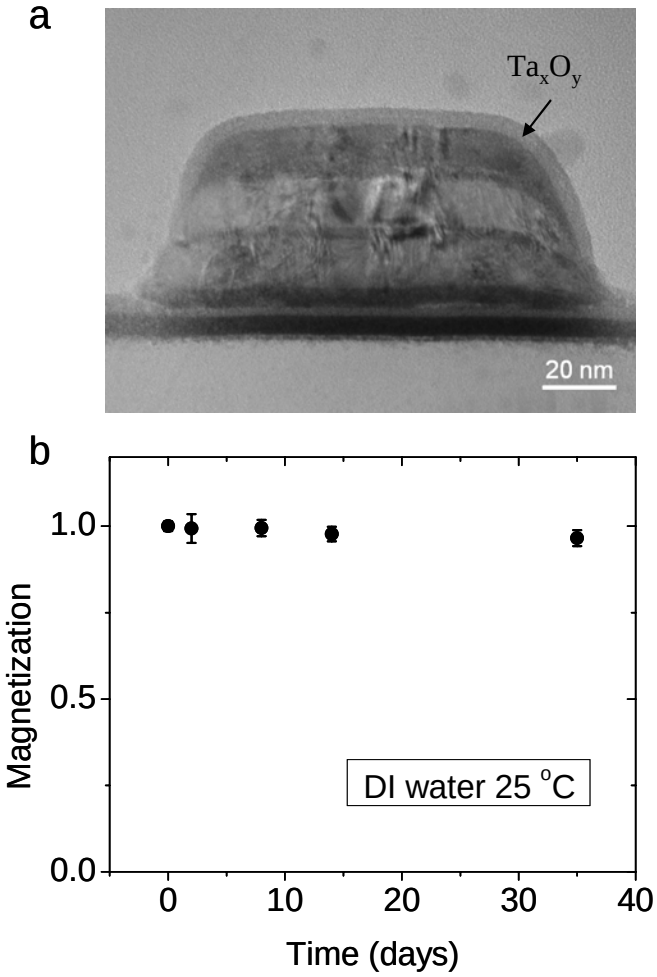

Figure S1. Passivation of SAF nanoparticles. a, Cross sectional TEM image of a single SAF nanoparticle on substrate. A thin layer of Ta_xO_y protects magnetic layers from oxidation and corrosion through sidewalls. **b,** A stability test of released SAF nanoparticles in de-ionized water at room temperature shows that the magnetization (normalized to the initial value) of SAF nanoparticles are very stable in water over one month.

Alternative stamp fabrication methods

We have demonstrated the feasibility of producing monodisperse nanoparticles with magnetic moments whose magnitude and field dependence can be adjusted over broad ranges. Obtaining large quantities of such particles at reasonable costs using advanced lithography techniques (such as interference lithography[1,2]) has been an active research area. In this context, we have developed a nanoimprint lithography (NIL) based fabrication method, derived from methods already in use to fabricate inexpensive optical compact disks. However, the fabrication of stamps using electron beam lithography, and the use of electroformed daughter stamps for production, remain high cost items which must be amortized over production volumes. Fortunately, in our simple application, there is no demand for precise spiral tracks, for incorporation of coding patterns with distinct feature sizes, or for nanometer-scale overlay between multiple device layers.

This permits the use of self assembly techniques to produce packed arrays of carboxylate-modified latex nanoparticles (CML) which serve as etch masks for production of pillar arrays covering 4” silicon wafers. An SEM image of a latex particle array (Fig. S2a), produced by spin coating 200 nm particles from a 4 % w/w aqueous suspension, shows hexagonally packed arrays with dislocations. The latex particle diameters are reduced by etching with an oxygen containing plasma (Fig. S2b) and this pattern is transferred into Si pillars by etching with NF_3, (Fig. S2c). The polydispersity is negatively affected by evident small features which are often associated with dislocations, but it is expected that this situation can be improved. The SAF nanoparticles made with this stamp have 70 nm diameters (Fig. S2d) and their magnetic properties are similar to those described in the main text, provided the magnetic film thickness is scaled to maintain the aspect ratio. By using this alternative to e-beam stamp fabrication, it is hoped that direct fabrication methods can become practical for low volume production.

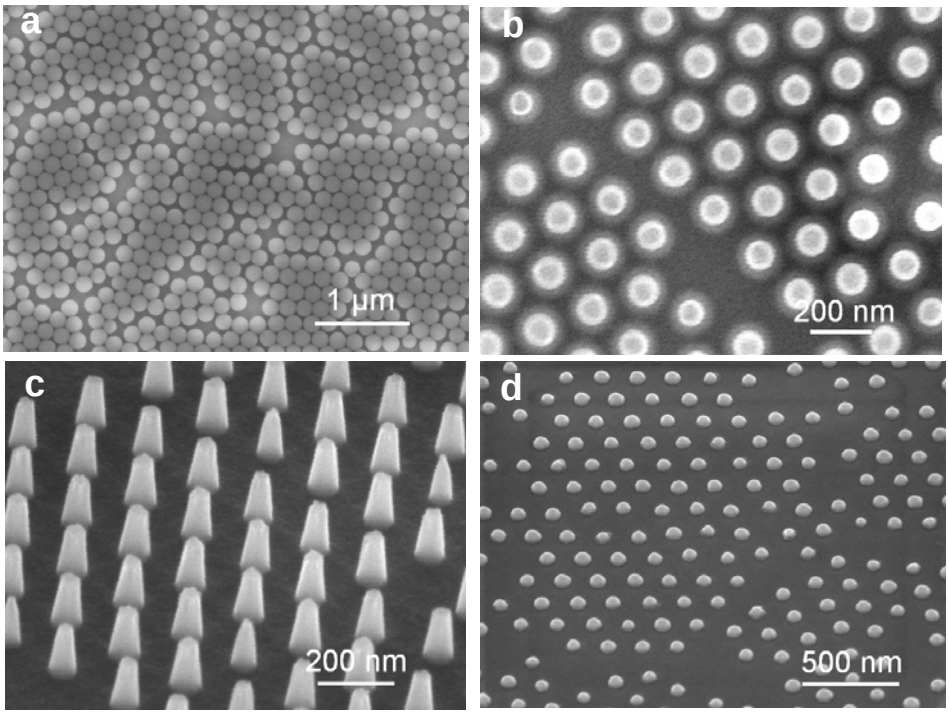

Figure S2. SEM images of particle production using self assembled stamps. a, Latex particles are spin coated onto a wafer. **b,** The particle diameter is reduced by oxygen plasma etching. **c**, The Si wafer is then selectively etched using an NF_3 plasma to produce pillars. **d**, Metal dot arrays are generated using self assembled stamps.

Reducing remanence by using SAF structure

In this work Ru is used as a nonmagnetic spacer layer in the SAF nanoparticles, and the remanence and coercivity of these nanoparticles are nearly zero (Fig. S3, C). If these same particles are produced using a single magnetic layer, the coercivity and remanence are dramatically increased (B), resulting in aggregation. These changes in magnetic properties are not simply associated with the magnetic material, but rather are consequences of patterning, as is evident in the low coercivity of continuous films (A).

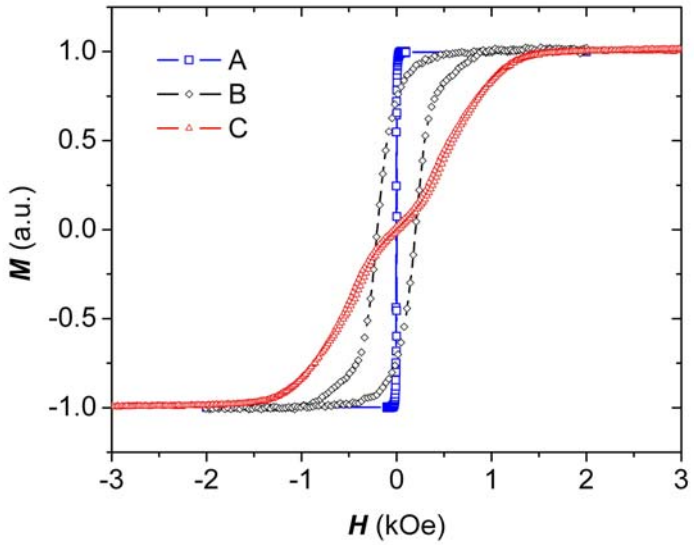

Figure S3. Hysteresis loops for a continuous magnetic film (A) , and films patterned into nanoparticles containing a single magnetic layer (B), and magnetic bilayers (C). The structures of the samples are given with layer thickness in nm:
A (blue): Ta(5)/Ru(2)/CoFe(12)/Ru(2)/Ta(5) continuous
B (black): Ta(5)/Ru(2)/CoFe(12)/Ru(2)/Ta(5) patterned, 120 nm
C (red): Ta(5)/Ru(2)/CoFe(6)/Ru(2.5)/CoFe(6)/Ru(2)/Ta(5) patterned, 120 nm

Characterization of SAF nanoparticles in solution

We use solution measurements to further elucidate the characteristics of freely suspended SAF nanoparticles. Magnetic hysteresis loops are obtained (Fig. S4) by enclosing 10 µL volumes of solution, containing about 10^8 particles, in paraffin containers attached to an AGM probe. Atomic concentrations are quantified using inductively coupled plasma-optical emission spectroscopy to determine the atomic components of the acid digested nanoparticles.

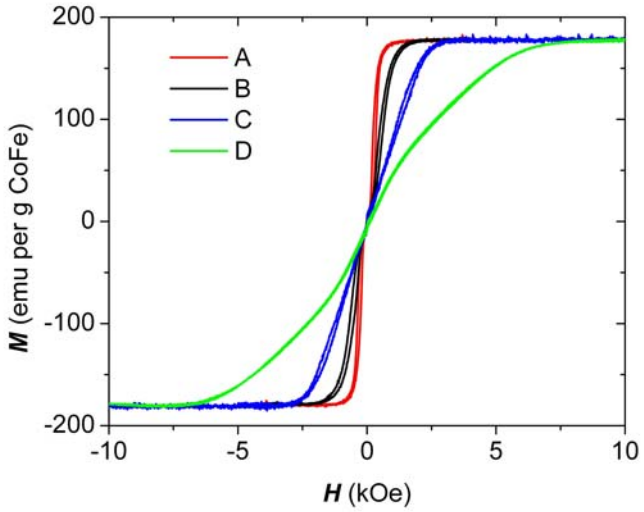

Figure S4. Magnetization versus applied field demonstrating control of saturation field for ~120 nm diameter SAF nanoparticles in aqueous solution (after release). The structures of the samples, listed from low to high saturation field, are given with layer thickness in nm:

A (red line): Ta(5)/Ru(2)/CoFe(6)/Ru(2.5)/CoFe(6)/Ru(2)/Ta(5);

B (black line): Ta(5)/Ru(2)/CoFe(12)/Ru(2.5)/CoFe(12)/Ru(2)/Ta(5);

C (blue line): Ta(5)/Ru(2) /CoFe(6)/Ru(0.6)/CoFe(6)/Ru(2)/Ta(5);

D (green line): Ta(5)/Ru(2)/$[CoFe(3)/Ru(0.6)]_3$ /CoFe(3)/Ru(2)/Ta(5).

Optical observations of SAF nanoparticles in solutions

SAF nanoparticles strongly scatter light, so they can be viewed and tracked using reflected light optical microscopy even though the nanoparticle size is well below the diffraction limit of the objective lens. Immersion oil is used to reduce the intensity of light reflected from the coverslip, which otherwise diminishes the nanoparticle contrast. Streams of images are acquired, with 40 ms exposures and 2/s frame rates, and averaged. The averaged data is used to correct for non-uniform illumination and gray scale levels are then adjusted until the reflected background appears nearly dark. Under these conditions numerous nanoparticles are evident, as shown in Fig. S5a. To continuously track individual nanoparticles, 0.5 μL of diluted solution was used between a glass slide and cover slip, which were pressed together repeatedly during optical imaging until the particles remained continuously visible. The gap, measured by focusing on glass surface defects, must be <4 μm. Brownian motion is quantified by digitizing tracks made by diffusing particles in the absence of an external field (Fig. S5b),

and calculating the average rms displacements as a function of the time between frames. The results allow the determination of drifts induced by solution flow and of the diffusion constant, D = 6 μm^2/sec, which agrees with the value calculated for 100 nm spheres (5 μm^2/sec). Magnetically induced velocity is similarly determined, but using lower magnification and large displacements to diminish diffusion effects. This motion is produced by positioning a small rotatable permanent magnet beneath the slide, to generate a field of 1 kOe and a gradient of 1 kOe/cm, which is reversed to check solution flow. Figure 3b in the Text showed data which gave a velocity v = 3 μm/sec. The expected field induced velocity is estimated, using Stokes viscous drag forces, from the formula $3\pi\eta D\mathrm{v} = V\nabla(\boldsymbol{M}\cdot\boldsymbol{H})$, to be 4 μm/sec; for 100 nm spheres with M = 1,700 emu/cm^3, t = 6 nm, D = 100 nm, η = 0.9 centiPoise, and V is the magnetic volume of the SAF nanoparticle.

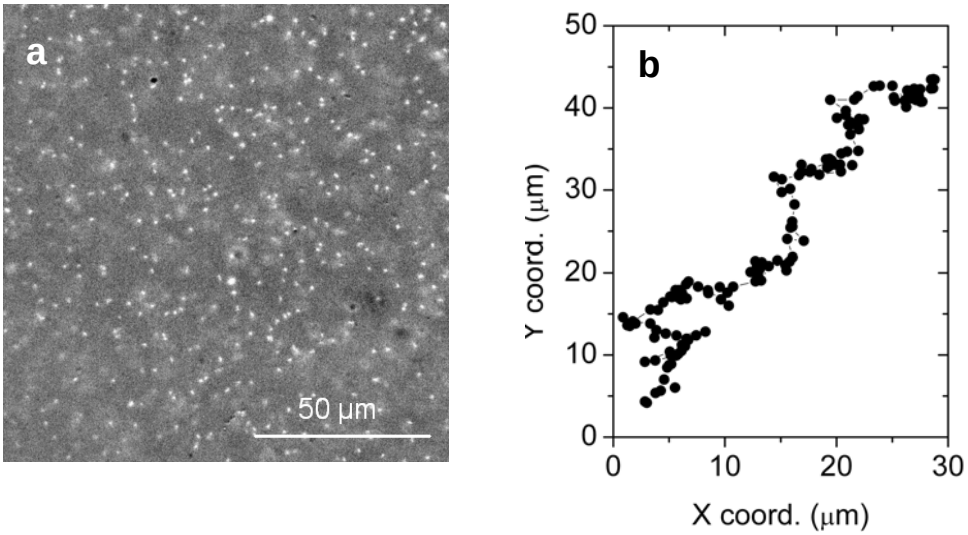

Figure S5. Optical observation of SAF nanoparticles in solution. a, Individual SAF nanoparticles in solution. **b,** Tracks of a single SAF nanoparticle in Brownian motion in the absence of an external magnetic field.

Detection of SAF nanoparticles with spin valve sensors

While this work is primarily aimed at demonstrating nanoimprinted high-moment antiferromagnetic nanoparticles with multiplex functionality, SAF nanoparticles can also be used for magnetic detection by spin valve sensors. The principle of spin valve sensors is published elsewhere (Ref. [26-28] of the main text). Our preliminary experiments indicate that the SAF nanoparticles can be detected by the spin valve sensors (data not shown) and thus are promising as magnetic labels in biodetection.

Because the saturation field of SAF nanoparticles can be tuned, conceptually SAF nanoparticles can be exploited for multiplex magnetic labeling. For example, consider a "two-color" or duplex scheme with two types of SAF nanoparticles with different saturation field, as shown in Fig. S6. Two measurements at different fields H_1 and H_2 are performed. The signals from SAF1 are the same as it is saturated in both cases, so the net difference of the two measurements gives an account of the number of SAF2 nanoparticles as the net change of magnetic signal per SAF2 nanoparticle from H_1 to H_2 is predetermined. The net signal of SAF1 nanoparticles can then be obtained by subtracting the signal due to SAF2 from the measurements at H_2, and the # SAF1 nanoparticles can then be counted as the net magnetic signal per SAF1 nanoparticle at H_2 is predetermined.

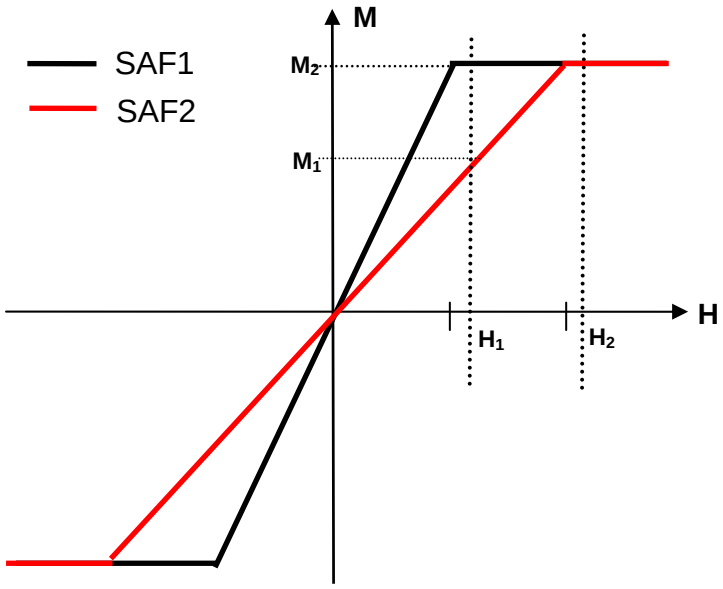

Figure S6. Schematic magnetic hysteresis loops of two types of SAF nanoparticles with different saturation fields. They can be used for duplex magnetic labeling of two distinct analytes in a biological sample as the number of each type of SAF nanoparticles can be unambiguously determined by two measurements at two different applied fields.

References

[1] C. A. Ross, M. Hwang, M. Shima, J. Y. Cheng, M. Farhoud, T. A. Savas, H. I. Smith, W. Schwarzacher, F. M. Ross, M. Redjdal, F. B. Humphrey, *Phys. Rev. B* **2002**, *65*, 144417.

[2] L. J. Heyderman, H. H. Solak, C. David, D. Atkinson, R. P. Cowburn, F. Nolting, *Appl. Phys. Lett.* **2004**, *85*, 4989.